Development of Digital Signal Processor Controlled Quantum Cascade Laser Based Trace Gas Sensor Technology

Stephen G. So, *Student Member, IEEE*, Gerard Wysocki, J. Patrick Frantz, *Member, IEEE*, and Frank K. Tittel, *Life Fellow, IEEE*

***Abstract*—This paper reports the design and integration of a custom digital-signal-processor (DSP) system into a pulsed quantum-cascade-laser (QCL)-based trace gas sensor to improve its portability, robustness, and operating performance. Specifically, this paper describes the implementation of a custom prototype DSP data acquisition and system controller based on the Texas Instruments TMS320F2812 for embedded control and processing. In addition, the sensor incorporates oversampling by taking advantage of the high-speed conversion capabilities of an analog-to-digital converter, which is embedded within the DSP. A carbon monoxide sensor, employing a thermoelectrically cooled, pulsed 4.6-μm distributed feedback QCL as a mid-infrared radiation source, is used to evaluate the performance characteristics of such a DSP controlled spectroscopic gas sensor.**

***Index Terms*—Data acquisition, digital signal processors (DSPs), pulsed lasers, semiconductor lasers.**

I. Introduction

INFRARED (IR) laser spectroscopy is a highly sensitive and selective technique for the real-time detection at part-per-billion (ppb) to part-per-trillion (ppt) concentration levels of molecular trace gases important in such diverse application areas as environmental and atmospheric sciences, chemical analysis, and industrial-emission monitoring as well as medical diagnostics, specifically the detection of exhaled breath biomarkers. Gas phase molecular compounds have a spectral fingerprint in the mid-IR from $\sim$ 3 to 24 μm. Environmental, industrial, and medical trace gases such as nitric oxide (NO), carbon monoxide (CO), ammonia (NH_3), methane (CH_4), and ethylene (C_2H_4) are distinguishable from each other due to the high specificity measurement capability of tunable pulsed and continuous wave (CW) coherent light sources that can inherently generate narrow linewidth mid-IR radiation [1]. A number of applications require sensor electronics for control, data acquisition, and management, which have an ultracompact footprint, provide flexibility and reliability and require low electrical power consumption.

Manuscript received August 26, 2005; revised January 17, 2006. This work was supported by the Physical Sciences Inc. (PSI), the National Aeronautics and Space Administration (NASA), the Texas Advanced Technology Program, the Robert Welch Foundation, and the Office of Naval Research via a subaward from Texas A&M University. The associate editor coordinating the review of this paper and approving it for publication is Dr. Erno Lindner.

The authors are with Department of Electrical and Computer Engineering, Rice University, Houston, TX 77005 USA (e-mail: steveso@rice.edu; gerardw@rice.edu; jpfrantz@rice.edu; fkt@rice.edu).

Digital Object Identifier 10.1109/JSEN.2006.881350

Various noise sources produce effects detrimental to the detection limit of pulsed quantum cascade laser (QCL)-based sensors. In order to mitigate these effects, various techniques can suppress noise, and thereby improve the minimum detection limit of a particular trace gas. This paper briefly explores noise sources and their methods of removal and determines the extent to which the noise has been suppressed electronically using a custom digital-signal-processor (DSP) solution as compared to commercial hardware.

II. Laser Absorption Spectroscopy (LAS)

LAS of target gas species, which is based on the Beer-Lambert absorption law, effectively determines real-time gas concentrations. Beer Lambert law states

$$I(\nu) = I_0 \cdot e^{-\alpha(\nu)\cdot L} \tag{1}$$

where I is the intensity of light passing through the absorbing medium, I_0 is the input intensity, L is the optical pathlength, ν is the radiation frequency, and $\alpha(\nu)$ is the absorption coefficient of a specific target species described by

$$\alpha(\nu) = C \cdot S \cdot g(\nu - \nu_0) \tag{2}$$

where C is number of molecules of the absorbing gas per unit volume [molecule cm^{-3}], S is the molecular line intensity [cm^{-1}/molecule $\times$ cm^{-2}], and $g(\nu - \nu_0)$ is the normalized lineshape function of molecular absorption [cm], which may be Gaussian, Lorentzian, or Voigt [1]. Typically, target absorbances $-\ln(I/I_0)$ at the level of 10^{-4} to 10^{-6} need to be measured in order to reach ppb to ppt sensitivity of C in the mid-IR spectral region.

A typical laser-based gas sensor consists of three key components: 1) most appropriate spectroscopic radiation source for the application; 2) either a simple or multipass cell used as an optical cavity to hold the target gas(es) and enhance the effective L; or the appropriate optics for an open path configuration; and 3) either a sensitive IR detector in the case of an absorption technique or a microphone/piezoelectric transducer in the case of photoacoustic spectroscopy.

The four most frequently implemented tunable CW mid-IR spectroscopic sources suitable for high-precision laser-based trace gas sensing are: 1) lead-salt laser sensors based on tunable group IV–VI lead-salt diode lasers [2]; 2) difference frequency generation (DFG)-based sources, which perform optical

frequency mixing of two near-IR telecommunications diode lasers in a nonlinear optical crystal [3]; 3) optical parametric oscillators (OPOs) [4]; and 4) solid state and QCLs [5]. For this paper, a mid-IR QCL-based LAS configuration offers ppb detection limits in a sensitive, compact gas sensor configuration.

The spectroscopic source of choice in many trace gas sensing applications is the QCL, due to its operating wavelengths in the mid-IR region, where the molecular spectral line intensities are significantly stronger (by a factor of $\sim$ 20 to 200) in comparison to overtone or combination spectral lines in the near-IR. In addition, pulsed and CW QC lasing capability at quasi-room temperatures are obtainable by means of thermoelectric (TE) cooling [6], [7]. A QCL also has the advantage of wavelength tunability by means of a current and temperature as well as external grating control [8], narrow linewidth, and a nonbandgap determined operating wavelength. Distributed-feedback (DFB) structures coupled to the QCL structure provide smoothly tunable single frequency operation [9].

III. Noise-Reduction Considerations

Noise sources such as absorption spectrum and electronic baseline fluctuations, acquisition/nonlinearity noise, pulse-to-pulse fluctuations, and detector noise are the main limiting factors for trace gas detection sensitivity in pulsed QC-LAS-based sensors. This section briefly discusses these noise sources, the way to reduce their influence, and an analysis of the various noise-suppression methods.

A. Noise Distributions

The most prevalent noise source in the sensor system described in this paper is white Gaussian noise. The distribution follows a probability density function (pdf):

$$f(x;\mu,\sigma) = \frac{1}{\sigma\sqrt{2\pi}} \exp\left(\frac{(x-\mu)^2}{2\sigma^2}\right) \tag{3}$$

where σ is the standard deviation and μ is the mean. When averaging a Gaussian distribution, the sample set size determines the sample standard deviation (s_N) and narrows the possible region of the true mean. The parameter (s_N) decreases as a function of $\sqrt{Hz}$ until the other noise sources dominate. Noise types other than Gaussian are difficult to remove. Switching noise can provide structured noise distributions due to its digital nature, generating strong harmonics. This noise usually couples into analog circuitry by crosstalk, grounding contamination, or electromagnetic-interference (EMI) emission if not properly shielded. The 1/f noise, another noise source, affects the accuracy of the resulting dc values from sample and hold, gated integration, or lock-in demodulation.

B. Gas Absorption Spectrum Baseline Fluctuations

Gas absorption spectrum baseline fluctuations occur from interfering species, which have spectral absorption features in the same wavelength region as the spectral line of the target species. To minimize gas baseline fluctuations, an interference free absorption line must be selected, and pressure broadening should be reduced. However, broadband absorbers are usually present in real-world applications, which cannot be avoided. Baseline measurement, subtraction or normalization eliminates such noise sources as long as the baseline is smooth across the spectral feature. One method to normalize the baseline is to perform a baseline fit to the wings of the spectrum where the absorption of the target gas is zero.

C. Electronic Baseline Fluctuations/Low Frequency Drift

Sensor power supplies and voltage regulators may fluctuate due to temperature and current loading effects. In addition, voltage references to digital-to-analog converters (DACs) and analog-to-digital converters (ADCs) also have a temperature coefficient (tempco, sometimes TC) drift, causing low frequency fluctuations. Lower tempco drift ratings for references and temperature stabilization for the electronic enclosure provide better low frequency performance. Baseline fluctuations also occur via the ubiquitous 1/f noise and are minimized by increasing frequency. The same baseline subtraction described above in Section III-B simultaneously removes some of the electronic drift. Frequent signal offset measurements (when the laser radiation is suppressed), and subtraction minimizes the influence of these noise sources.

D. Single-Pulse and Pulse-to-Pulse Fluctuations

The measurements of identical laser pulses differ due to electronic noise, temperature drift, timing jitter, and movement of optical elements. When the pdfs of these sources are convoluted, the final statistical distribution is close to a Gaussian distribution (central limit theorem). Thus, a more efficient reduction of noise is accomplished via an increase in pulse rate or an increase in the number of spectral averages. The QCL driver may also have difficulty in providing constant amplitudes (1–2 A) of current pulses with durations of 10–20 ns, and hence, the QCL output power fluctuates "pulse-to-pulse." This effect is removed by pulse normalization, usually accomplished optically via a beamsplitter to provide both a sample and reference channel. This type of noise may also be used to naturally provide dithering of the signal, which is usually applied to reduce quantization noise.

E. Acquisition Noise and Nonlinear System Response

Acquisition noise originates from noise sources such as EMI, crosstalk, noise from voltage references and power supplies, timing jitter, and quantization noise. Noise from these sources as well as noise created by nonlinearity of the system response can vary in distribution, and averaging these distributions can cause measurement errors.

Removing these sources requires targeted electronic design efforts. The layout of the printed circuit board (PCB) can have a large effect on EMI and crosstalk between traces, which is solved using various PCB layout design rules. Noise from voltage references and supplies can be reduced by using low-noise versions and filtering. Parts with better power-supply-rejection-ratio (PSRR) ratings diminish the effect of power-supply ripple. Nonlinearity (differential and integral nonlinearity—DNL and INL) depends on the choice of ADC. Effects of DNL can be

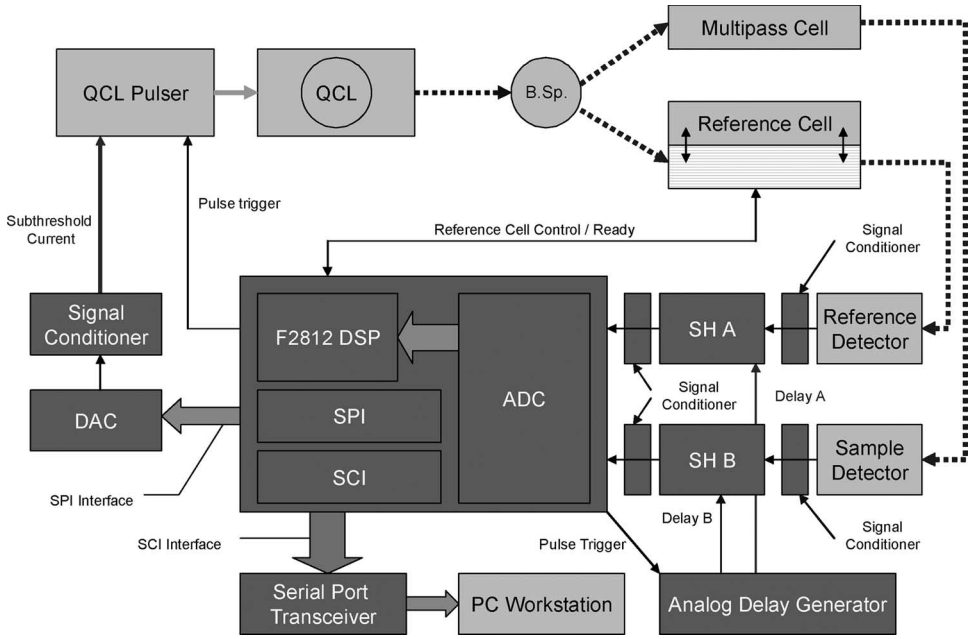

Fig. 1. Block diagram depicts control electronics of a QCL-based gas sensor. The DSP provides high-speed control, signal generation, and signal acquisition for sensor components.

minimized by a sufficient dither, and INL can be removed by calibration.

Timing jitter is another type of acquisition noise, which is important in synchronous detection schemes. With narrow detected pulses, the slope of the signal is large; therefore, if the acquisition clock has a large amount of jitter, the noise will increase. This type of noise is only avoided by using low-drift and low-jitter electronic timing components, or can be minimized by averaging of a larger number of pulses. However, stable timing sources are available, and as long as the jitter is much less than the width of the detected pulse, the jitter acquisition noise will be minimal.

Some acquisition noise may be reduced by oversampling the signal, since usually, a single normalized point is sampled from each pulse. The uncorrelated noise for the sample and reference channels for a single pulse cannot be removed unless the sample size is sufficient. Noise levels theoretically should decrease by $\sqrt{n}$, where n is oversampling depth if acquisition noise is present. Increasing the number of oversampling points per pulse either by increasing hold time or higher sampling speed may improve the signal to noise ratio (SNR).

F. Detector Noise

Noise from the detector causes error in the sampled signals. Minimizing the effect of detector noise requires more pulses for a larger sample set or higher optical powers. Both techniques help to suppress background fluctuations, which are unrelated to the laser radiation, such as electronic noise or excitation of the detectors by stray radiation.

IV. DSP-Based Gas Sensor System Platform

A custom developed DSP platform based on the Texas Instruments Inc (TI). TMS320F2812 provides faster sampling in order to more effectively minimize noise and baseline fluctuations in spectroscopic applications compared to a previous QC-LAS sensor using a National Instruments Inc. DAQCard-6062E 12-bit PCMCIA card. In addition, the custom electronics incorporate signal conditioning, data acquisition, data processing, and control systems in order to provide compact size and independent operation. The DSP selected provides adequate processing power to perform all the necessary functions for autonomous and real-time operation. More processing resources and faster wavelength sweeps allow the instrument to recognize fluctuations and perform appropriate corrections. Bomse *et al.* reported a TI TMS320C6701 DSP-based sensor that uses a CW vertical cavity surface emitting laser (VCSEL) at 6395.43 cm^{-1}, which is capable of a minimum CO detection limit of $\sim$ 25 ppm [10]. A C6X DSP platform was also considered for the reported platform, but the F2812 was eventually selected based on both size and cost.

Fig. 1 depicts a block diagram of the basic control electronics for a pulsed QCL-based gas sensor. This sensor consists of a custom designed PCB mated to a Spectrum Digital Inc. eZdsp F2812 evaluation module (EVM). The sensor system offers a generalized platform suitable for a TE-cooled pulsed QCL-based sensor. Multichannel GPIO pins act as control outputs for various sensor functions (e.g., triggering and gas handling). Two ADC channels were reserved for pulsed detector signals, leaving the remaining 14 channels for other system parameters (such as temperature and pressure). The embedded nonvolatile flash memory on the DSP stores the system software programming. After power up, the DSP self-boots from flash and commences running system code. Thus, this sensor can operate independently of any external personal or single board computer. The combined daughtercard and EVM electronics have a small form factor of $16.6 \times 7.6 \times 3.8$ cm and are "instant-on" (marginal boot time). An embedded standard RS232 universal asynchronous receiver-transmitter (UART) (Maxim MAX3223) and an embedded Ethernet controller (Cirrus Logic

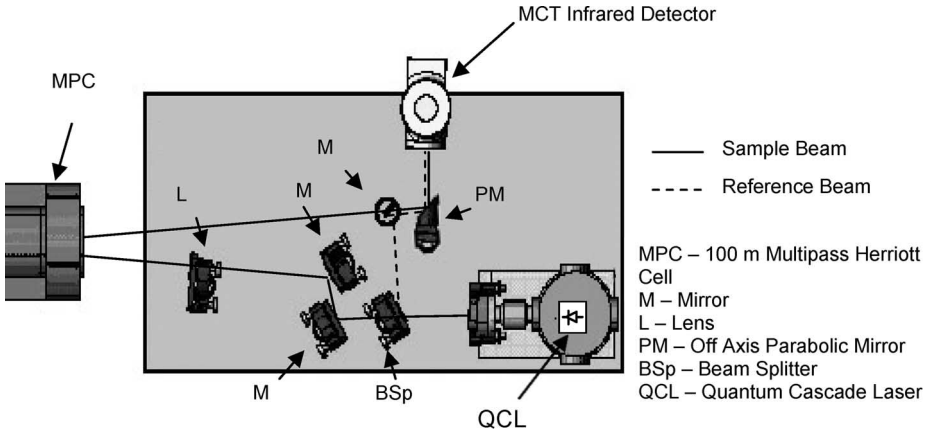

Fig. 2. Optical configuration of a 4.6-μm CO QCL sensor with a 100-m astigmatic Herriott cell. A beam splitter generates signal and reference beams for pulse normalization.

CS8900A) provide the system with external communications options. Wireless connectivity and control via translation of RS232 UART to IEEE 802.11 G wireless Ethernet allowed for a remote download by a computer with wireless Internet access. Such wireless capability coupled with autonomous operation allows for functionality, where human intervention is undesirable, such as in medical quarantine areas or in harsh environmental conditions.

A. Optical and Electronic Configuration of QCL-Based Trace Gas Sensor

A QCL mounts on a two-stage Peltier cooler inside an evacuated vacuum housing to prevent water condensation at QC substrate temperatures below the dew point. In order to minimize pulse-to-pulse fluctuations, a beamsplitter divides QCL power into sample and reference beams, and laser pulse power normalization is performed to improve the SNR in the measured spectrum [11]. The reference beam is directed to the detector, while the sample beam first passes through an astigmatic Herriot multipass cell (MPC) [12] prior to being incident on the same detector. The detected signal and reference pulses are distinguishable due to the time required to pass through the 100-m effective optical path length of the MPC. Both the sample and reference beams are combined and focused onto a Mercury-Cadmium-Telluride (MCT) detector (Kolmar Tech., model: MPV8-1-J1-DC) (see Fig. 2) via an off-axis parabolic mirror with a 7.62-cm (3 inch) focal length. The QCL has a total tuning range of ~ 10 cm^{-1} from 2171–2181 cm^{-1}, which is achievable by scanning the temperature of the QC chip within a range between -30 °C and 0 °C (measured at the heat sink). The QCL is capable of targeting three CO spectral lines [13]: The R(7), R(8), and R(9) lines (Fig. 3), which are free of interference from other species. The R(8) line at 2176 cm^{-1} corresponds to a maximum QCL output power at a moderate Peltier cooler temperature (-22 °C) and is interference free from H_2O lines. A measure of the instrumental linewidth, which is determined using deconvolution of a spectrum recorded from a known reference CO mixture, yields ~ 0.02 cm^{-1} (~ 600 MHz).

Current pulses of 750 mA with a 23-ns long duration and a maximum 1.0-MHz pulse rate (corresponding to the maximum recommended duty cycle by the laser manufacturer) provide an injection current to the laser with a threshold current of 600 mA. This provides an average optical power of ~ 0.05 mW. The QCL wavelength is scanned by a modulation of the subthreshold current using a saw-tooth waveform. At the end of each scan, the laser pulse trigger is disabled, which causes suppression of the laser output and allows collection of an offset value for each channel. A serial peripheral interface (SPI) provides an effective and robust interface to control a two-channel TI TLV5638 DAC for generation of arbitrary modulation waveforms (Fig. 1). The TLV5638 specifies a settling time of 1 μs and an update rate of 233 kilosamples per second (KSPS), which is fast enough to provide a voltage step suitable for 1-MHz pulse rates. The modulation waveform in this paper employs a saw-tooth waveform with 233 values/scan at a 1-kHz sweep rate. An amplifier/filter follows the DAC, removing quantization noise before the waveform feeds a subthreshold current modulation circuit. With short QCL pulses of ~ 20 ns, the bandwidth of the detector signal is much greater than the maximum sampling rate. Complete recovery of the detector signal (20-MHz bandwidth using KMPV8-1-J1-DC Kolmar MCT detector) would be possible at two times the bandwidth $=$ 40 MHz (Nyquist Criterion). However, the ADC sampling rate of 12.5 megasamples per second (MSPS) is much less than the Nyquist rate, and continuous digitization of the detector signal is not possible for this system. For that reason, we use a dedicated external two-channel sample and hold (SH) circuit with a timing scheme to synchronize the sampling with the arrival of optical pulses to assure peak amplitudes of the signal extracted from each pulse. Synchronization is possible via a phase matching of the "hold" signal supplied to the SH circuit with the periodic amplitude peaks of the detector signal to assure sampling of maximum values. The remainder of the analog front end provides a matched gain to the DSP ADC input signal range.

The complete front end consists of three modules: multivibrator (integrated circuits) ICs with RC time constant-based timing delays, an external SH to capture and hold a value of the pulse signal, and conditioning amplifiers to match to the full scale input range of the ADC. An inverting amplifier based on a low-noise high-bandwidth op-amp provides the required attenuation of the SH output, and it performs a first-order low

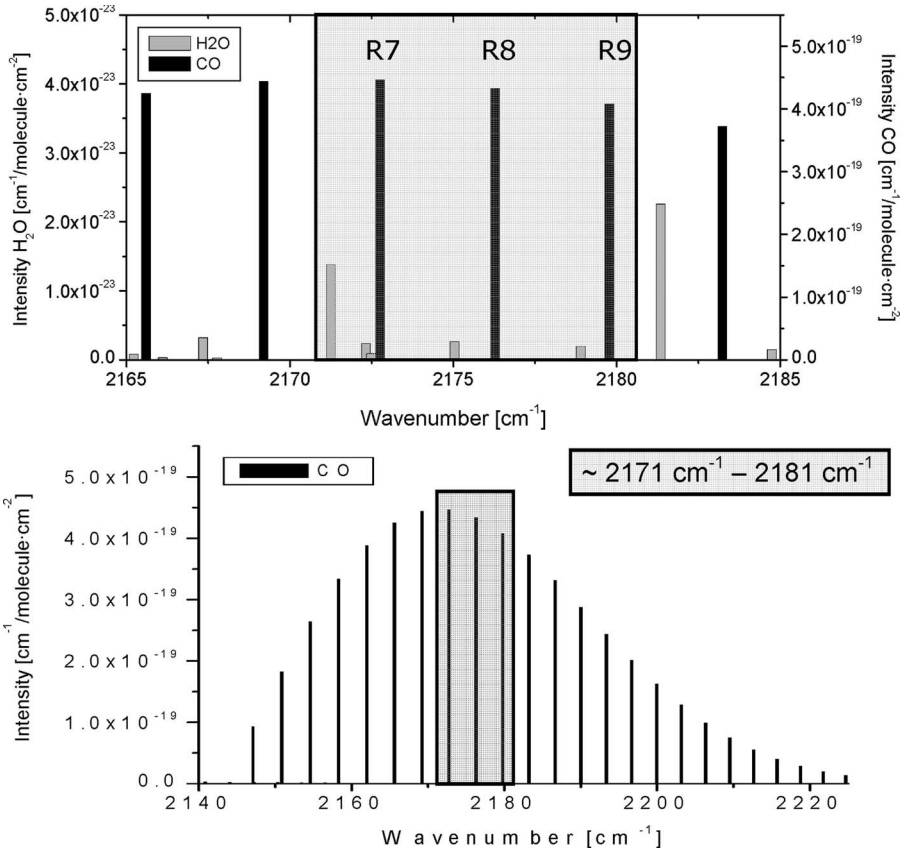

Fig. 3. Carbon monoxide absorption lines accessible by a 4.6-μm QCL. The QCL has a thermal tuning range of 10 cm^{-1} and can target the R(7) to R(9) lines of CO, which are interference free from water absorption lines.

pass filtering in order to suppress high frequency noise at the input of the ADC. The embedded ADC simultaneously samples both channels at its single-ended inputs with a resolution of 12 bits over 3 V.

Fig. 4 shows the electronic and optical signal traces generated by the pulsed QCL sensor. The timer-compare signal (generated by the event manager clock circuitry integrated in the DSP IC) provides triggering of the laser pulse. The custom delay generator controlled by the trigger signal produces a clock signal with appropriate delay and duty cycle to synchronize the SH ICs to the current pulse. The DSP event manager, in addition to controlling the clock circuitry, also synchronizes the ADC sequencer in order to measure the points for oversampling at identical times within one laser pulse cycle. This assures that when the ADC takes offset measurements, the ADC measures the same harmonic fluctuations.

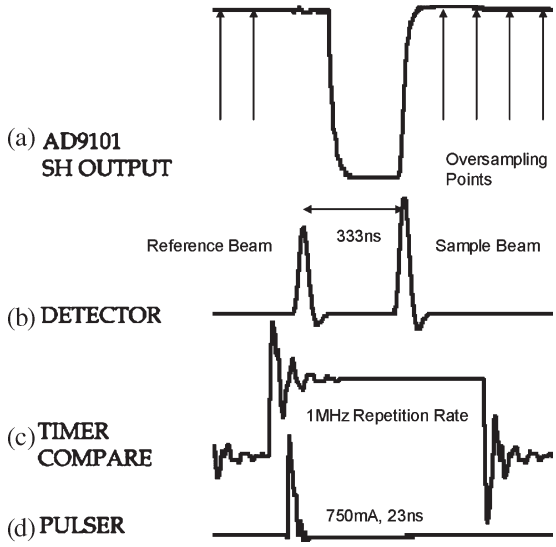

Fig. 4. (a) SH output signal is oversampled at multiple points to reduce acquisition system noise. Traces of optical and electronic signals for data acquisition. The DSP timer circuitry compares the event manager clock register with a compare register to produce the (c) "timer compare" signal to trigger the (d) current pulses, and a single detector receives both signal and reference beam pulses, which are distinguishable by (b) time delay.

B. Software Development

A combination of C programming language and TMS320F28X assembly languages provided ease of programming the processing algorithm (C), and high execution efficiency for time-critical routines and interrupts (assembly). Texas Instruments Code Composer Studio DSK v2.21 provides an integrated development environment (IDE) and compiles, assembles, and flashes the machine code to program memory.

A 12.5-MHz timer clock derived from the 150-MHz PLL CPU clock rate drives an interrupt-based algorithm. This clock provides synchronization for data acquisition and signal generation. When the embedded event manager timer count register (EVAT1CNT) reaches a programmed value (EVAT1CMP) [14], the system triggers a pulse. The system continues counting up until the timer matches a period register (EVAT1PR), which

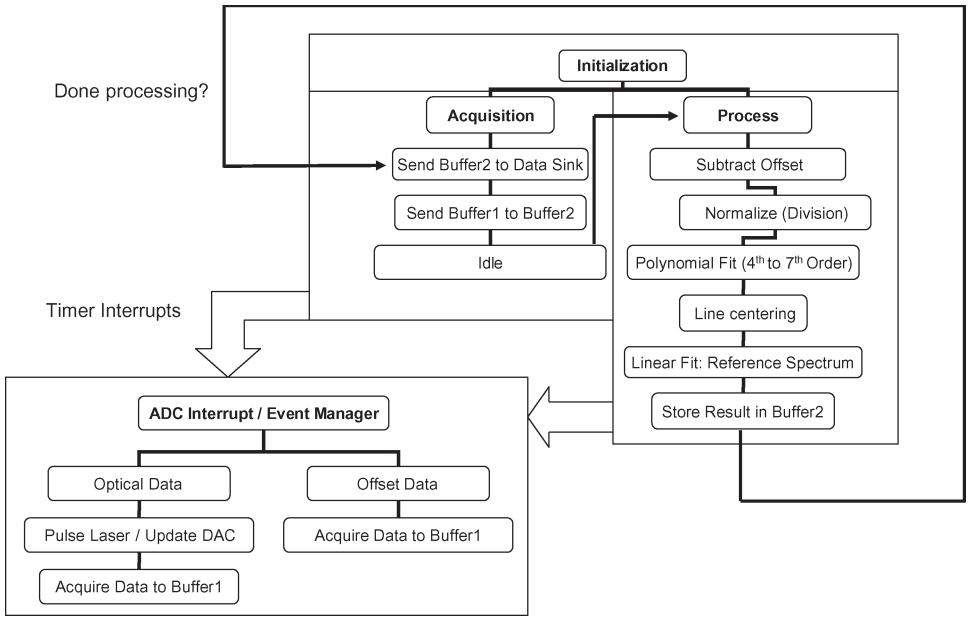

Fig. 5. DSP software program flow diagram. The DSP acquires data to one memory buffer using a timed interrupt, while the system performs calculations in the background on another memory buffer.

then triggers the ADC sequencer to start conversion. The ADC sequencer permits the system to convert a short stream of simultaneous data points with a single start of conversion signal, which this system exploits for oversampling.

A generic polynomial fitting routine, which is based on Gauss-Jordan elimination [15], allows for high-speed baseline fitting and concentration calculations, providing fast execution times and low memory usage in a processing-resource-scarce and memory-scarce environment. The software is programmed to solve the overdetermined system of equations

$$A^T A x = A^T b \tag{4}$$

where

$$A = \begin{bmatrix} 1 & \nu_1 & \cdots & \nu_1^{n-1} \\ \vdots & \nu_2 & \cdots & \nu_2^{n-1} \\ \vdots & \vdots & \cdots & \vdots \\ 1 & \nu_m & \cdots & \nu_m^{n-1} \end{bmatrix} \tag{5}$$

$$b = \begin{bmatrix} y_1 \\ \vdots \\ y_m \end{bmatrix} \quad \text{and} \tag{6}$$

$$x = \begin{bmatrix} c_1 \\ \vdots \\ c_n \end{bmatrix} \tag{7}$$

for m pairs of measured gas absorption (y) versus frequency (v) data points, and $c_1 \ldots c_n$ are coefficients for the fitted polynomial

$$p(\nu) = c_1 + c_2\nu + \cdots + c_n\nu^{n-1}. \tag{8}$$

Improvement of the polynomial fitting performance allows the system to process a spectrum more frequently, avoiding the slowest fluctuations, and increasing temporal resolution.

The generalized polynomial fitting algorithm also performs first-order linear fits with a spectrum of a known gas sample. The calibration gas spectrum stored in a processor memory provides values for comparison with the sample gas spectrum. The DSP computes the slope of the best linear fit of the function

$$y_{\mathrm{s}}(\nu_{\mathrm{i}}) = f\left(y_{\mathrm{r}}(\nu_{\mathrm{i}})\right) \tag{9}$$

where y_{s} and y_{r} represent absorption data at frequency ν_{i} for a sample and reference gas, respectively. The calculated slope determines the comparison factor for calculating the sample gas concentration. Electronic drifts can cause slight detuning of the laser frequency. In order to assure that the absorption lines are in the correct position within the scan for comparison, the software monitors the line positions and shifts the spectra when necessary. With each integer position number shift, the fitting algorithm calculates a new slope (c_2) and determines the overall minimal offset (c_1) for each of ± 5 points of the initial line center position. Fig. 5 shows the overall interrupt-based software algorithm, which acquires data to memory buffers and transforms the spectral measurements to gas concentration values.

V. Results

In previous work [16], the QCL pulse rate was the limiting factor in reducing the noise level to achieve a minimum trace gas detection limit. Using the DAQCard-6062E data-acquisition card with the same electronic hardware and software configuration as in [16], the presented CO optical sensor with the 100-m MPC (see Fig. 6) is able to achieve 6 ppb in 3 s. The DAQCard uses a maximum of 500-KSPS sampling rate spread over four channels (two detector channels, two offset channels) with one pair of samples per pulse, resulting in a 125-kHz pulse rate.

The daughtercard is capable of producing a control waveform to pulse the laser at up to 6 MHz, with a maximum sampling

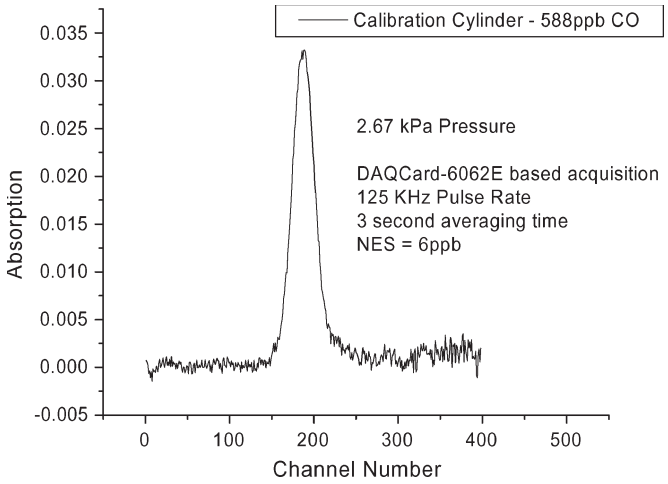

Fig. 6. CO absorption line at 2176 cm^{-1} acquired using a DAQCard-6062E. Normalized NES is 6 ppb (in 3 s) and a 125-kHz pulse rate. Signal showed $\sim 3.3 \times 10^{-4}$ noise level with a signal of ~ 0.0322 resulting in a 97.6 SNR.

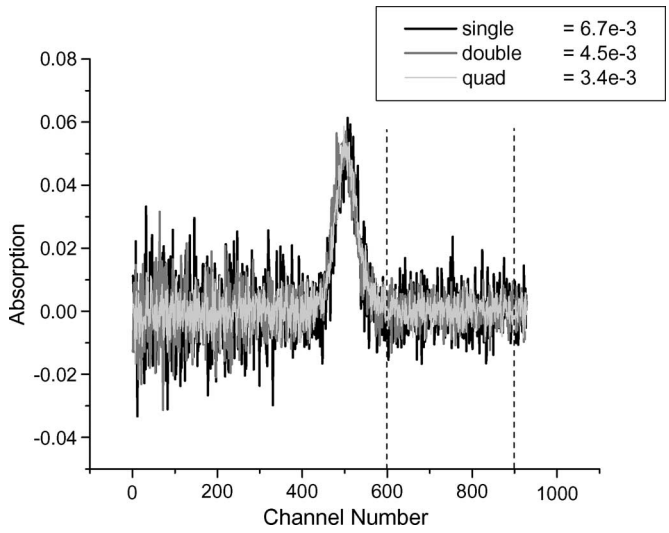

Fig. 7. Oversampling reduces acquisition-system noise by increasing the number of data samples taken from a single pulse. The noise is white (Gaussian distribution) in nature as shown by the $\sqrt{n}$ dependence on the standard deviation of noise in the spectral wings of a CO spectrum acquired by the DSP system, where n is the oversampling depth.

rate of 12.5 MSPS. Laser drivers that provide such high repetition rates at high pulse currents and low pulse duration are not commercially available. Therefore, to exploit the fast data-acquisition capability of the system, the ADC oversamples the pulses [17] by holding the pulse value using the SHs and collecting multiple ADC conversions (at the highest ADC speed possible) from the same pulse value. This reduces the acquisition-system noise, so that the ratio of sample to reference signal from a single pulse is more accurate in a single shot. Oversampling is possible by using any method, which can increase the duty cycle of the signal, such as triggering external SH ICs with delay generators (as in this paper) or by performing gated integration of the signal.

The average power dissipated within the laser chip changes due to the changes in duty cycle while varying the repetition rate of the laser current pulses. Therefore, the temperature of the laser changes, causing the emitted wavelength to shift, which modifies the operating point of the laser (parameters such as laser threshold current), defining the limits of comparison. By varying pulse rates between 202 and 403 kHz (Table I), the CO absorption line shifts within the scan but is still within the scanning range. Additionally, an observable change in peak laser current occurs due to capacitor bank charging time constant effects of the laser driver. For the aforementioned range of pulse rates, a drop of 37.3 mA (from 795 mA) occurs, reducing the measured optical signal from 5.75 to 3.80 V measured at the output of the MCT detector (66% of the available optical signal). Multiplying the 403-kHz noise level (0.463) by 0.66 gives a value of 0.305, which is comparable to the 0.294 noise level of the 202-kHz spectra. Thus, the single spectrum inferred noise levels are equal, assuming similar parameters of the optical signal.

Table I also shows the results of the test used to determine oversampling versus a single sampling performance, which reveals improvements in the acquired SNR for oversampling. The test was performed using a reference gas to acquire spectra. Noise levels were determined using the standard deviation of the baseline wings. Using a 202-kHz pulse rate with a double oversampling and 1613 spectral averages, a spectral noise level of $\sigma_{1613^*2} = 5.18 \times 10^{-3}$ was observed. The inferred noise level of a single point is $\sigma_1 = \text{sqrt}(1613^*2)^*5.18 \times 10^{-3} = 0.294$. The same was performed with a 266-kHz pulse rate with a quad over sampling that yielded a result of $\sigma_{2127^*4} = 3.5 \times 10^{-3}$ and $\sigma_1 = 0.323$. These values for noise levels were obtained using the same acquisition time (8 s), in order to assure that the same amount of time is allowed for low frequency baseline fluctuations affecting the measurement. Higher repetition rates caused a greater single point noise level (σ_1) due to reduced optical power, but the overall averaged noise level improves. Oversampling provided the correct Gaussian noise reduction (see Fig. 7), which demonstrates that the oversampling is beneficial and can overcome the problem of a limited laser pulse rate.

Determination of timing jitter in the acquisition system is useful, since oversampling does not remove this noise source. The steps taken in this measurement are as follows: 1) The data acquisition system determines the overall pulse shape to find the average slope of one of the pulse edges. This is done by measuring a 0.1-V, 20-ns pulse with 1-MHz repetition rate generated by a low jitter pulse generator (Stanford Research SRS DG535) and varying the phase in 1-ns increments (Fig. 8), 2) acquiring data for each point and analyzing statistically to determine the standard deviation of the measured signal, and 3) determining the jitter using the deviation of the signal measured in the center of the rising edge of the pulse at the phase delay of 2 ns. The standard deviation ($\sim$ 1.67 mV) measured at this point, combined with the slope (0.06 V/ns) of the edge, demonstrates 28 ps of jitter, a value low enough for this application.

Using the highest available pulse rate/oversampling, the DSP stand-alone system reveals an improvement in the noise equivalent sensitivity (NES). A CO spectrum taken from a pure mountain air (from Niwot Ridge, Colorado with known CO concentration of 126 ppb), by performing a triple oversampling at 1.042 MHz, shows a 6.3-ppb NES in 0.96 s (see Fig. 9). Additionally, an absorption spectrum of a 588-ppb CO in N_2

TABLE I
SINGLE SPECTRUM INFERRED NOISE LEVELS FOR VARIOUS PULSE RATES AND OVERSAMPLING LEVELS. THE HIGHER VALUE OF NOISE AT 403 kHz WAS DUE TO A DECREASE IN PULSE CURRENT AVAILABLE AT HIGHER REPETITION RATES

Pulse Rate (Hz)	Spectral Averages (X)	Over-sampling Level (Y)	Noise Level(σ_{X*Y})	Inferred Noise Level (σ_{1})
201,612	1613	2	0.00518	0.294
265,957	2127	1	0.00650	0.300
265,957	2127	4	0.00350	0.323
403,225	3226	1	0.00816	0.463 (0.305)

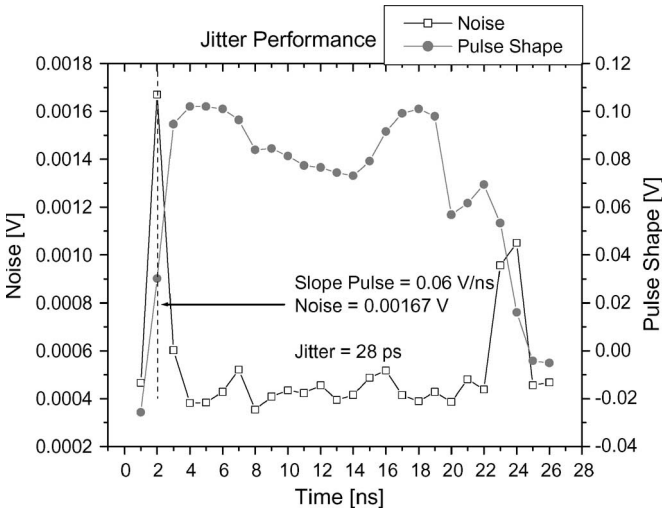

Fig. 8. Jitter measurement provides the trigger-to-trigger timing accuracy of the sampling clock. The rising edge slope and the noise are used to determine the jitter (28 ps) of the analog delay generator.

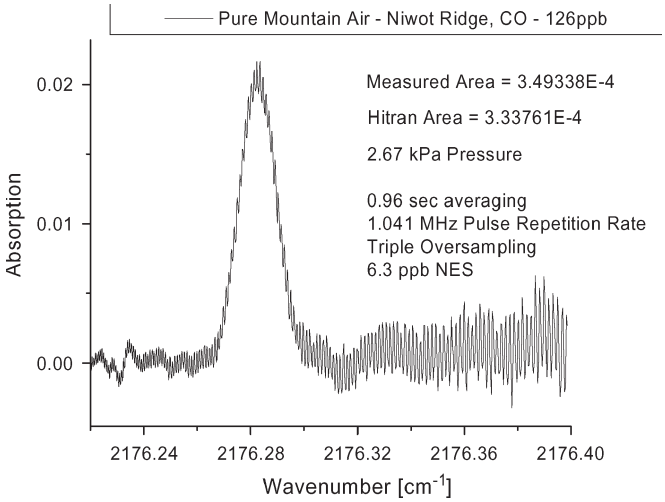

Fig. 9. Carbon monoxide absorption spectrum of pure mountain air at 2.67 kPa from Niwot Ridge, CO containing 126-ppb CO. The data acquisition settings for the 4.6-μm QCL sensor are a 1.042-MHz pulse rate, triple oversampling, and 0.96-s averaging. The measured noise level was $\sim 1 \times 10^{-3}$, which yields a NES of $\sim$ 6.3 ppb.

reference mixture acquired with the same parameters is shown in Fig. 10. The resulting noise level matches the value in Fig. 9. Utilization of the ADC converter embedded in the DSP is currently 6.25 MSPS out of the maximum 12.5 MSPS during autonomous real-time operation, which is 50% of its capability due to programming constraints (Fig. 11). Fig. 12

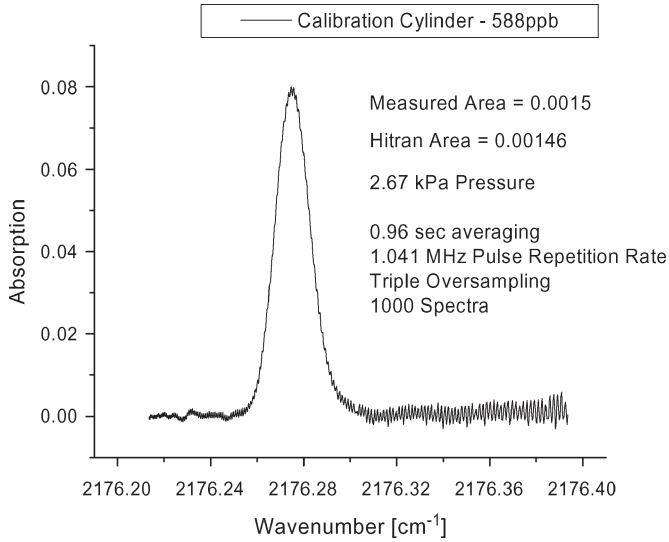

Fig. 10. Absorption spectrum of a 588-ppb CO : N_2 mixture at 2.67 kPa acquired with a 1.042-MHz pulse repetition rate, triple oversampling, and 0.96-s averaging. Noise levels match those of Fig. 9.

illustrates theoretical noise reduction, assuming an identical signal stability over 8 s. The curves were generated using the $\sqrt{Hz}$ dependence of the noise. The measured data presented in this paper follow the theoretical trends.

The dominating noise in this system was found to be ADC noise pickup. To confirm this, the daughterboard was detached from the DSP EVM, and the ratio between channels shunted to ground by a 50 Ω load was measured. In this configuration, the same noise behavior was observed. DSP analog/digital power coupling and EMI effects on the eZdsp evaluation board are the primary sources of this noise. Fig. 13 illustrates the generated noise spectrum measured at the input of the ADC using a network analyzer (Stanford Research SRS SR760). When the processor is running through its pipeline and actively fetching and executing instructions, the digital noise and emitted radiation from the processor cause an integrated 100-kHz bandwidth noise level of 0.219 V at the analog input pins.

Although this is a substantial noise level, the sensor provides detection limits, which exceed the NI DAQCard 6062E-based system by overcoming the noise with faster sampling. The DAQCard-based acquisition system applied to the CO sensor achieves a NES of 6 ppb in 3 s (500 spectra, 750 point spectrum), as compared to the DSP system with NES of 6 ppb in 1 s (1000 spectra, 1000 point spectrum, triple oversampling). Due to double mode laser operation effects observed for the DAQCard sensor architecture at the lower pulse rate of 125 kHz (compared to the DSP pulse rate of 1.042 MHz) and higher

(a)

```
C code                          Assembly Pseudocode

while(foo)                      Load bar
{                               Branch Conditional:bar (7 cycles)
        if(bar)                 Load foo
         updateDAC();           Branch Conditional:foo (7 cycles)
}                               Load bar
                                Branch Conditional:bar
```

(b)

```
C code (unrolled)               Assembly Pseudocode (unrolled)

while(foo)                      Load bar
{                               Branch Conditional:bar (7 cycles)
        if(bar)                 Load bar
         updateDAC();           Branch Conditional:bar (7 cycles)
        if(bar)                 Load foo
         updateDAC();           Branch Conditional:foo (7 cycles)
}                               Load bar
                                Branch Conditional:bar
```

(c)

```
C code (interrupt)              Assembly Pseudocode (interrupt)

while(foo)                      Load bar
{                               Branch Conditional:bar (7 cycles)
        if(bar)                 ** interrupt ** (?? cycles)
         updateDAC();           Load bar
** interrupt **                 Branch Conditional:bar (7 cycles)
        if(bar)                 Load foo
         updateDAC();           Branch Conditional:foo (7 cycles)
}                               Load bar
                                Branch Conditional:bar
```

Fig. 11. DSP processor architecture and its compulsory programming has an effect on timing. (a) Polling is slow due to branch instructions. (b) Loop unrolling improves flag polling performance. (c) Interrupts cause a variable number of cycles delayed before the next poll of the flag.

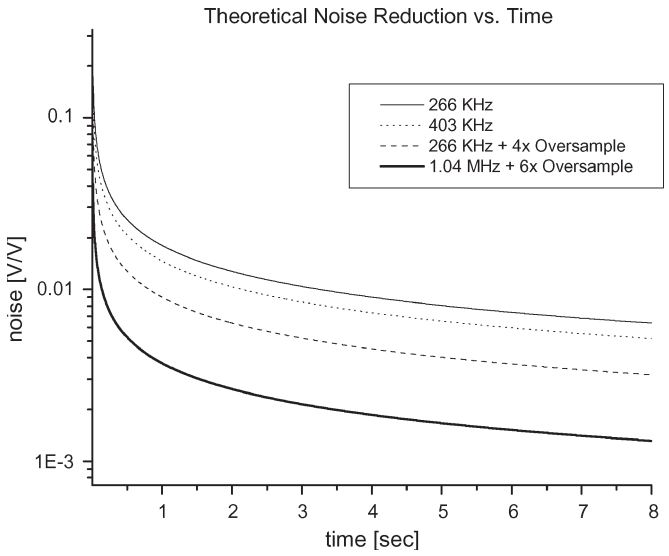

Fig. 12. Theoretical noise reduction is shown from a single-spectrum noise level of 0.300 V/V for various pulse rates and oversampling depths, assuming the same noise behavior as the slowest acquisition settings. 1.042 MHz with six times oversampling of two channels (12.5 MSPS) is the theoretical limit of the TMS320F2812 DSP-based hardware.

peak current above threshold, the calculated absorption signal is lower in Fig. 6 than in Fig. 10. However, a comparison of noise levels with normalized absorption signals shows similar SNR (see Fig. 14) in a shorter acquisition time. The average optical power measured with the DSP controlled system at the high laser pulse repetition rate was only $\sim$ 12% of the power available for the DAQCard experiment; in spite of this, an improvement of more than 40% (from 10.4 ppb/$\sqrt{Hz}$ to 6 ppb/$\sqrt{Hz}$) was achieved for the DSP-based instrument.

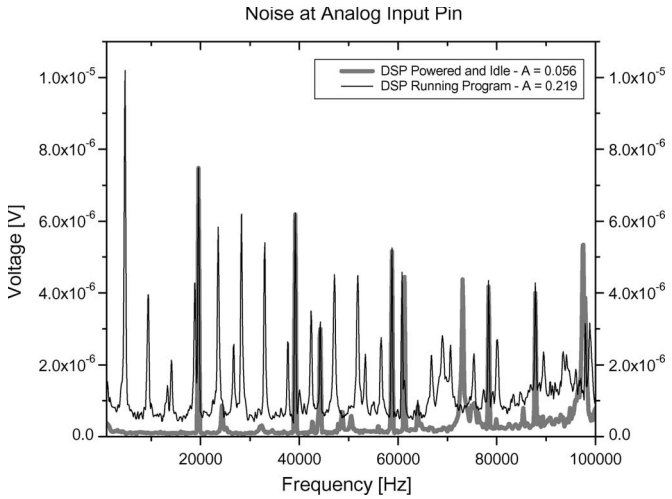

Fig. 13. Network analyzer noise spectrum at the analog input pin of an eZdsp TMS320F2812 EVM (Rev. C). The noise increases when the DSP processor is actively processing instructions due to digital noise feedthrough/EMI/EMC.

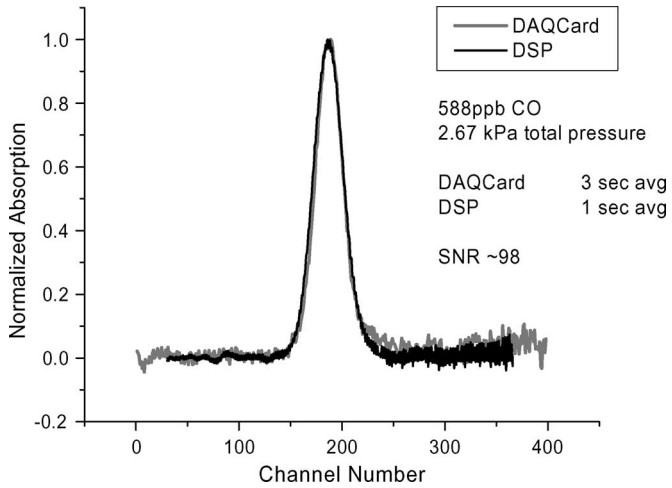

Fig. 14. Comparison of DAQCard-6062E and DSP daughtercard approach shows similar noise levels with less averaging time for greater temporal resolution. Both solutions obtain an SNR of $\sim$ 98. The spectra are the same spectra from Figs. 6 and 10. The channel number scale for the DSP was adjusted to match the DAQCard scale.

Another advantage to oversampling is a lowered overall current draw for lasers, which require high power current pulses. Pulsing the laser with more pulses and running each of these pulses through the full analog front end would take more power than using solely electronic techniques to artificially create more data points. Hence, reducing the number of pulses required while maximizing the SNR is the optimum methodology for low power pulsed sensor systems (especially portable systems). For the CO sensor described here, at threshold currents, the laser draws $\sim$ 100 mW of power at 1 MHz. Assuming the laser accepts pulses at 3 MHz with the same pulsewidth and current, the system would draw $>$ 300 mW in excess of the analog electronics, while three times oversampling reduces the same amount of noise using only the analog electronic power.

The embedded software can perform real-time autonomous monitoring of CO in laboratory air over a period of time. Fig. 15 shows the test results of the system measuring ambient gas samples by setting a flow controller to a 2.67 kPa (20 Torr)

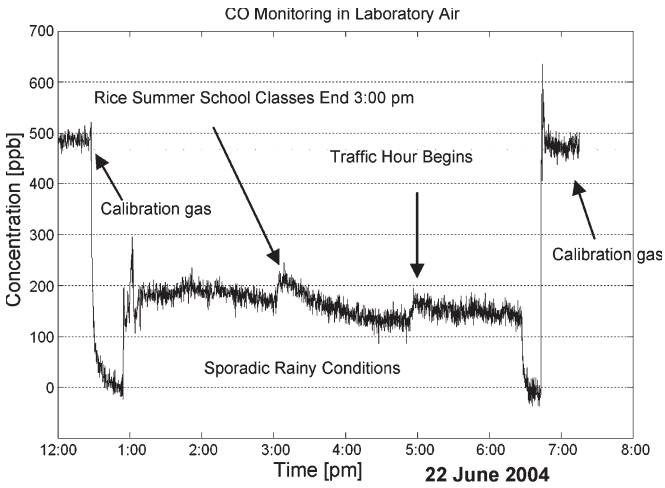

Fig. 15. Continuous CO monitoring test of the DSP controlled QCL-based gas sensor system. Precision was $\sim$ 40 ppb at a 125-kHz QCL pulse rate with no oversampling. This measurement was taken as a first trial of the system (before noise optimization) as a baseline for comparison.

set point to sample the ambient air over an 8-h period, and continuously pumping the MPC. The spikes in CO at $\sim$ 3:00 and $\sim$ 5:00 PM correlate with on-campus traffic outside of the laboratory. Calibration gas spectra taken before and after the test demonstrate consistent values.

VI. Conclusion

A QCL-based sensor with DSP technology demonstrates PC-independent processing, while simultaneously improving detection limits electronically. Integrated electronic systems reduce the overall system footprint, and significantly simplify system operation. Software developed for high-speed sampling and processing for real-time autonomous implementation requires further optimization to take full advantage of the architecture.

With higher oversampling (six times at 1.042-MHz pulse rate for a dual channel, resultant 12.5-MHz sampling rate) after further software optimization and a custom noise reducing implementation not reliant on the commercial EVM, dedicated analog power supply, high-precision low-drift components, stronger power supply decoupling, and/or cleaner mixed signal layout techniques [18] should further improve attainable trace gas detection limits electronically.

References

[1] F. K. Tittel, D. Richter, and A. Fried, "Mid-infrared laser applications in spectroscopy," in *Solid-State Mid-Infrared Laser Sources*, vol. 89, I. T. Sorokina and K. L. Vodopyanov, Eds. Berlin, Germany: Springer-Verlag, 2003, pp. 445–510.

[2] J. Chen, S. So, H. Lee, M. P. Fraser, R. F. Curl, T. Harman, and F. K. Tittel, "Atmospheric formaldehyde monitoring in the greater Houston area in 2002," *Appl. Spectrosc.*, vol. 58, no. 2, pp. 243–247, Feb. 2004.

[3] D. G. Lancaster, A. Fried, B. Wert, B. Henry, and F. K. Tittel, "Difference-frequency-based tunable absorption spectrometer for detection of atmospheric formaldehyde," *Appl. Opt.*, vol. 39, no. 24, pp. 4436–4443, Aug. 2000.

[4] D. Costopolous, A. Miklos, and P. Hess, "Detection of N_2O by photoacoustic spectroscopy with a compact, pulsed optical parametric oscillator," *Appl Phys. B*, vol. 75, no. 2/3, pp. 385–389, Sep. 2002.

[5] A. A. Kosterev and F. K. Tittel, "Chemical sensors based on quantum cascade lasers," *IEEE J. Quantum Electron.—Special Issue QC Lasers*, vol. 38, no. 6, pp. 582–591, Jun. 2002.

[6] A. A. Kosterev, R. F. Curl, F. K. Tittel, R. Köhler, C. Gmachl, F. Capasso, D. L. Sivco, and A. Y. Cho, "Transportable automated ammonia sensor based on a pulsed thermoelectrically cooled quantum-cascade distributed feedback laser," *Appl. Opt.*, vol. 41, no. 3, pp. 573–578, Jan. 2002.

[7] D. Weidmann, F. K. Tittel, T. Aellen, M. Beck, D. Hofstetter, J. Faist, and S. Blaser, "Mid-infrared trace-gas sensing with a quasicontinuous-wave Peltier-cooled distributed feedback quantum cascade laser," *Appl. Phys. B*, vol. 79, no. 7, pp. 907–913, Nov. 2004.

[8] G. Wysocki, R. F. Curl, F. K. Tittel, R. Maulini, J. M. Bulliard, and J. Faist, "Widely tunable mode-hop free external cavity quantum cascade laser for high resolution spectroscopic applications," *Appl. Phys. B*, vol. 81, no. 6, pp. 769–777, Oct. 2005.

[9] A. A. Kosterev, R. F. Curl, F. K. Tittel, C. Gmachl, F. Capasso, D. L. Sivco, J. N. Baillargeon, A. L. Hutchinson, and A. Y. Cho, "Effective utilization of quantum-cascade distributed-feedback lasers in absorption spectroscopy," *Appl. Opt.*, vol. 39, no. 24, pp. 4425–4430, Aug. 2000.

[10] D. S. Bomse, D. C. Hovde, S. J. Chen, and J. A. Silver, "Early fire sensing using near-IR diode laser spectroscopy," in *Proc. SPIE—Diode Lasers and Applications in Atmospheric Sensing*, 2002, vol. 4812, pp. 73–81.

[11] D. Weidmann, A. A. Kosterev, C. Roller, R. F. Curl, M. P. Fraser, and F. K. Tittel, "Monitoring of ethylene by a pulsed quantum cascade laser," *Appl. Opt.*, vol. 43, no. 16, pp. 3329–3334, Jun. 2004.

[12] J. B. McManus, P. L. Kebabian, and M. S. Zahniser, "Astigmatic mirror multipass absorption cells for long-path-length spectroscopy," *Appl. Opt.*, vol. 34, no. 18, pp. 3336–3348, Jun. 1995.

[13] L. S. Rothman, A. Barbe, D. C. Benner, L. R. Brown, C. Camy-Peyret, M. R. Carleer, K. Chance, C. Clerbaux, V. Dana, V. M. Devi, A. Fayt, J.-M. Flaud, R. R. Gamache, A. Goldman, D. Jacquemart, K. W. Jucks, W. J. Lafferty, J.-Y. Mandin, S. T. Massie, V. Nemtchinov, D. A. Newnham, A. Perrin, C. P. Rinsland, J. Schroeder, K. M. Smith, M. A. H. Smith, K. Tang, R. A. Toth, J. Vander Auwera, P. Varanasi, and K. Yoshino, "The HITRAN molecular spectroscopic database: Edition of 2000 including updates through 2001," *J. Quant. Spectrosc. Radiat. Transfer*, vol. 82, no. 1–4, pp. 5–44, Nov./Dec. 2003.

[14] *TMS320x281x DSP Event Manager (EV) Reference Guide*, Texas Instruments Inc., Dallas, Texas, Texas Instruments Literature Number: SPRU065C, Nov. 2004.

[15] W. Press, *Numerical Recipes in C : The Art of Scientific Computing*. Cambridge, U.K.: Cambridge Univ. Press, 1992.

[16] G. Wysocki, M. McCurdy, S. So, D. Weidmann, C. Roller, R. F. Curl, and F. K. Tittel, "Pulsed quantum-cascade laser-based sensor for trace-gas detection of carbonyl sulfide," *Appl. Opt.*, vol. 43, no. 32, pp. 6040–6046, Nov. 2004.

[17] R. Lyons and R. Yates, "Reducing ADC quantization noise," *Microw. RF*, vol. 44, no. 6, p. 72, 2005.

[18] B. C. Baker. (2004, May). Analog circuit noise sources and remedies, *Electron. Compon. News*. [Online]. Available: http://www.ecnmag.com/article/CA418799.html

Stephen G. So (S'02) was born in 1981, in Houston, TX. He received the B.S. and M.S. degrees from the Department of Electrical and Computer Engineering, Rice University, Houston, in 2003 and 2005, respectively. He is currently working toward the Ph.D. degree at the same university.

He is currently with the Rice Laser Science Group. His current research interests are development of ultra compact, autonomous trace gas sensors, and their applications. In addition, he is also interested in the development of trace gas sensor networks and their applications.

Mr. So is a member of the Optical Society of America (OSA).

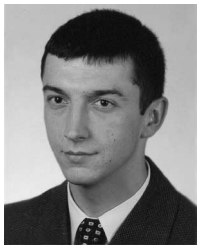

Gerard Wysocki was born in Jelenia Gora, Poland, in 1974. He received the Masters degree in electronics from the Wroclaw University of Technology, Wroclaw, Poland, in 1999 and the Ph.D. degree in physics from Johannes Kepler University, Linz, Austria, in 2003.

His Ph.D. research from 1999 to 2000 in the Department of Applied Physics at the Johannes Kepler University was focused on the application of near-field optics in laser induced chemical processing. In August 2003, he joined the Laser Science Group in the Department of Electrical and Computer Engineering, Rice University, Houston, TX. His current research interests are focused on various molecular absorption spectroscopy techniques used for detection of trace gases in environmental, industrial, medical, and fundamental science applications as well as development of new tunable laser sources suitable for performing of high-resolution molecular spectroscopy. He has published eleven papers in various technical journals and coauthored 31 presentations in both U.S. and international conferences and meetings.

J. Patrick Frantz (M'97) was born in Houston, TX, in 1973. He received the Bachelors degree in history, German, and political science, and the Masters degree in electrical engineering all from Rice University, Houston, in 1995 and 1997, respectively.

After graduation, he worked with Compaq Computer, where he designed motherboards for high-end PC servers. Following his experience in industry, he spent time as an Electrical Engineer and Programmer for the Human Genome Sequencing Center at Baylor College of Medicine, Houston, where he worked on numerous projects in the area of laboratory automation, embedded systems, and bioinformatics. Since 1999, he has been working with Rice University, where he is currently the Executive and Technical Director of the Center for Multimedia Communication, an institution devoted to theoretical and experimental research of next generation wireless communications systems. He also serves as the Director of the Electrical and Computer Engineering Industrial Affiliates program. In addition, he is a Lecturer on the ECE faculty and served as a Visiting Lecturer with the Tokyo Institute of Technology, Tokyo, Japan, in July 2005. He teaches several courses on embedded systems design and programming. His research interests include–but are not limited to–novel DSP and FPGA-based hardware systems, mobile wireless devices, and communications algorithm implementations. Finally, he has a passion for international engineering education and helping students to prepare for the global marketplace, and toward this end, he serves as Rice University's Special Liaison for international engineering education.

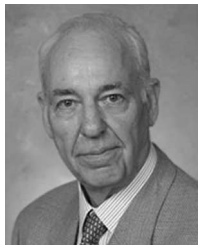

Frank K. Tittel (SM'72–F'86–LF'03) was born in Berlin, Germany, in 1933. He received the Bachelors, Masters, and Doctorate degrees in physics from the University of Oxford, Oxford, U.K., in 1955 and 1959, respectively. He also received a Doctor of Science (HC) degree from JATE University, Szeged, Hungary, in 1993.

From 1959 to 1967, he was a Research Physicist with General Electric Research and Development Center, Schenectady, NY. At General Electric, he carried out early pioneering studies of dye lasers and high-power solid state lasers. Since 1967, he has been with the Faculty of the Department of Electrical and Computer Engineering, Rice University, Houston, TX, where is currently an Endowed Chair Professor. He held Visiting Professor appointments with NASA Goddard Space Flight Center, University of Aix-Marseille, Keio University, Keio, Japan, Swiss Institute of Technology (ETH-Zurich). His current research interests include various aspects of quantum electronics, in particular, laser spectroscopy, nonlinear optics, and laser applications in environmental monitoring, process control, and medicine. He has published more than 300 technical papers and holds eight U.S. patents in these areas.

Dr. Tittel is a Fellow of the Optical Society of America and the American Physical Society. He is an Associate Editor of Applied Physics B and a former Editor-in-Chief of the IEEE JOURNAL OF SELECTED TOPICS IN QUANTUM ELECTRONICS (1996–1998) and is now Associate Editor of the same journal. He has served on numerous technical program committees such as CLEO, IQEC, and QELS for OSA and APS. In 1973 and 1981, he was an Alexander von Humboldt Senior Fellow at the Max-Planck Institutes of Biophysical Chemistry, Göttingen, Germany, and Quantum Optics, Munich, Germany, respectively.